Exploring interfacial reactions and optical properties of ZBLAN-based phosphor-in-glass color converters via spark plasma sintering for laser-driven lighting

Mengmeng Meng, Panyi Wang, Xiaoyu Hu, Manman Zhang, Binying Yang, Youjie Hua, Muzhi Cai, Laurent Calvez, Xianghua Zhang, Shiqing Xu

Exploring Interfacial Reactions and Optical Properties of ZBLAN-Based Phosphor-in-Glass Color Converters via Spark Plasma Sintering for Laser-Driven Lighting

Mengmeng Meng [a], Panyi Wang [a], Xiaoyu Hu [a], Manman Zhang [a], Binying Yang [c], Youjie Hua [a], Muzhi Cai [a, *], Laurent Calvez [b], Xianghua Zhang [b], Shiqing Xu [a]

[a] *Key Laboratory of Rare Earth Optoelectronic Materials and Devices of Zhejiang Province, Institute of Optoelectronic Materials and Devices, China Jiliang University, Hangzhou 310018, China*

[b] *ISCR (Institut des Sciences Chimiques de Rennes) UMR 6226, Univ Rennes, CNRS, F35000 Rennes, France*

[c] *Yinling School, Zhejiang Financial College, Hangzhou 310018, China*

Abstract: Phosphor-in-glass (PiG) is extensively utilized as a color converter in laser-driven lighting. Despite its popularity, a noteworthy concern is the potential for interfacial reactions to occur between the phosphors and the glass matrix during high-temperature processing, leading to subsequent corrosion. Previous research suggests that spark plasma sintering (SPS) may effectively limit these reactions in silica glass-based PiGs. However, the reactivity of silica glass, lacking glass modifiers, towards phosphors is diminished, raising uncertainty about whether SPS can truly fabricate a PiG with improved interfacial morphology. Nonetheless, research pertaining to PiG fabrication using SPS with multi-component glass compositions remains scarce. In this study, an attempt is made to address this gap by employing a multi-component glass matrix - ZrF_4-BaF_2-LaF_3-AlF_3-NaF (ZBLAN), which is known for its high reactivity with phosphors, in the creation of PiGs through SPS. $Lu_3Al_5O_{12}:Ce^{3+}$ (LuAG) was embedded within ZBLAN glass, fabricated using SPS in merely 5 min at a temperature of 255 °C. The subsequent analysis focused on the interfacial microstructure and the optical properties of the thus prepared PiG samples. The results demonstrate that the lower-temperature and time-efficient sintering process of SPS successfully mitigate the interfacial reactions between the phosphor and the glass matrix. Consequently, a

commendable luminous flux of 597 lm and luminous efficacy of 242 lm/W is achieved.

***Keywords**:* Phosphor-in-glass; $Lu_3Al_5O_{12}$: Ce^{3+}; SPS; Laser-driven lighting

1 Introduction

Light-emitting diodes (LEDs) have attained substantial recognition in the lighting and display sectors in recent years due to their superior luminous efficiency, extended lifespan, energy efficiency, and environmental sustainability [1-5]. However, a significant challenge known as "Efficiency droop" compromises LEDs' luminous efficiency at higher power densities, making them unsuitable for high-power solid-state lighting [6, 7]. Contrarily, laser diodes (LDs) can effectively circumvent this efficiency droop issue [8, 9]. Consequently, the technology of fluorescent conversion white laser diodes, based on blue laser diode-excited fluorescent materials—commonly referred to as laser-driven lighting technology—is anticipated to become the subsequent generation of lighting technology, succeeding LED lighting.

Nevertheless, the high photon flux laser beam produced by LDs can generate intense heat, surpassing the tolerance threshold of traditional organic encapsulation materials, which may cause damage to the phosphor [10]. To mitigate this problem, researchers are exploring the development of inorganic encapsulation materials for phosphors as a replacement for traditional organic materials, such as silicone [11-21]. Transparent inorganic glass [22-24] is considered a promising encapsulation material for phosphors in LD lighting due to its superior stability, affordability, and adjustable luminescence.

Phosphor-in-glass (PiG) inorganic color converters, employing transparent glass as the matrix and phosphors as the secondary phase [25,26], have received considerable attention as a promising material for lighting applications. Nonetheless, the high-temperature processing needed for inorganic glass consolidation can instigate interfacial reactions between the glass matrix and phosphors, leading to their corrosion.

Solid-phase sintering emerges as a promising and feasible approach to fabricating PiG materials exhibiting superior optical performance. Nonetheless, achieving low sintering temperatures coupled with abbreviated processing durations poses substantial challenges. Spark plasma sintering (SPS) is an innovative solid-phase sintering

technique capable of realizing fully dense glass materials at relatively low temperatures within minimal timescales, effectively circumventing issues inherent to conventional melt-quenching methodologies [27].

Wang et al. [28] successfully encapsulated $Y_3Al_5O_{12}$:Ce phosphor within silica glass via SPS at a temperature of 1000 °C. Their findings suggest that the restricted sintering process, characterized by its low temperature and brief duration, limited interfacial reactions, resulting in a PiG demonstrating remarkable luminous efficacy of 127.9 lm/W. Contrarily, Qiu et al. [29] recently reported extraordinary performance of a PiG material derived from a pressureless melting process at 1250 °C, using a silica glass matrix. It was observed that the silica glass matrix-based PiG exhibited no interfacial reaction, which they attributed to the absence of alkali and alkaline earth metals within the silica glass network. This revelation suggests that the meticulous regulation of sintering conditions inherent in the SPS process may not constitute the principal factor contributing to the minimal interfacial reaction observed in the study of Wang et al. [28]. Consequently, further investigation is warranted to fully comprehend the mechanisms involved in the fabrication of these advanced materials.

The effectiveness of the SPS process in producing PiG with superior interface morphology can be determined through an approach that involves the use of a multi-component glass matrix, containing alkali or alkaline earth metals, in the preparation of PiGs via SPS. Despite encouraging outcomes from SPS-based PiG reported in literature, research on the fabrication of PiG using SPS with multi-component glass compositions remains scarce. This study seeks to explore the potential of SPS process sintering conditions to inhibit the occurrence of interfacial reactions between phosphors and the multi-component glass matrix. ZrF_4-BaF_2-LaF_3-AlF_3-NaF (ZBLAN) glass, containing alkali or alkaline earth metals along with highly reactive fluoride ions, is selected as the matrix. If SPS can limit the interfacial reaction between ZBLAN glass and phosphors, it can potentially prevent or mitigate interfacial reactions in other glass compositions. $Lu_3Al_5O_{12}$: Ce^{3+} (LuAG) phosphors were selected due to their high luminous efficiency and excitation capability when stimulated by a 450 nm blue laser [30-32].

This study aims to investigate the impact of heating rate and sintering temperature on the transmittance of ZBLAN glass during the SPS process. Additionally, the fabrication of LuAG-PiG through SPS is examined, and the microstructure and interfacial morphology are analyzed using scanning electron microscopy (SEM) and transmission electron microscopy (TEM). The low-temperature rapid sintering process successfully produced LuAG-PiG samples with remarkable luminous flux (597 lm) and luminous efficiency (242 lm/W). Furthermore, the incorporation of $CaAlSiN_3$: Eu^{2+} (CASN) phosphor introduced a red component, allowing the development of a laser-driven white lighting device with a high color rendering index (89.8) and low color temperature (3354 K). These findings indicate that careful regulation of the sintering conditions during the SPS process can effectively minimize or eliminate the interfacial reaction between ZBLAN glass and phosphors, thereby enhancing the overall device performance.

2 Experimental

2.1 Sintering parameters

The parameters for generating dense and transparent ZBLAN glass through SPS were identified by conducting a series of reaction-sintering tests. ZBLAN glass was initially ground into a powder, with a particle size ranging between 3-5 μm, using an agate mortar in the absence of solvent media. The ground glass powder was carefully vacuum-packaged for backup purposes. Subsequently, 1.5 g of this glass powder was introduced into a carbon die, containing an aluminum foil barrier to deter carbon diffusion. This die underwent sintering in a vacuum using the SPS device (SPS-3T-3-MIN (H), provided by Shanghai Chenhua Technology Co., Ltd.).

Two sets of sintering process parameters were examined. In the first set, the sintering temperature was maintained at 255 ℃, and the heating rate was altered to 5 ℃/min, 20 ℃/min, 40 ℃/min, 60 ℃/min, 80 ℃/min, and 100 ℃/min. The samples generated from this process were named Z1 through Z6, respectively. In the second set, the heating rate was held constant at 40 ℃/min, while the sintering temperature was adjusted to 245 ℃,

248 ℃, 250 ℃, 253 ℃, 255 ℃, and 258 °C, yielding samples named Z7 through Z12, respectively. During the sintering process, the pressure and power are maintained at 0.5 t and 25% respectively.

2.2 Preparation of PiGs

Commercial LuAG phosphors (spherical shape), obtained from Jiangmen Keheng Industrial Co. Ltd., were amalgamated with the glass powders in concentrations varying from 1% to 10%. This mixture, with particle sizes of 3-5 μm for ZBLAN and 10-20 μm for LuAG, was ground in an agate mortar for 15 min without any solvent medium. The blend was then sintered in a graphite die and punch under vacuum conditions using the SPS device (SPS-3T-3-MIN (H), Shanghai Chenhua Technology Co., Ltd.). The sintering process consisted of several stages: the heating rate was set to 40 ℃/min, and the sintering temperature was held at 255 ℃. Once this temperature was achieved, it was sustained for a 5-min duration. Concurrently, the uniaxial pressure progressively increased from 100 °C, remaining at 0.5 t throughout the sintering process. The samples, named LuAG-PiG, were polished post-sintering and evaluated for a variety of properties. Finally, ZBLAN glass powder was combined with commercial LuAG and CASN phosphors, procured from Jiangmen Keheng Industrial Co. Ltd. The concentration of CASN phosphors was varied as follows: 7.5% LuAG-x% CASN (x=0.25%, 0.3%, 0.35%, 0.4%, 0.45%). This mixture underwent sintering, following the same procedure as applied to the LuAG-PiGs within the SPS process.

2.3 Characterization of the PiGs

The photoluminescence (PL) spectra of the prepared samples were acquired using a FL3-211 spectrometer (HORIBA, Jobin Yvon, France). The crystalline structure of the R-PiG samples was assessed by X-ray diffraction (XRD) utilizing a D8 Advance instrument (Bruker, Germany), with Cu Kα radiation operating at 40 mA and 40 kV, scanning an angle range of 20° to 80°. Sample transmittance was quantified with a UV-3600 UV-visible spectrophotometer (Shimadzu) within the wavelength range of 200-

800 nm. Quantum efficiency (QE) was gauged via an intensified multichannel spectrometer (QE-2100, Otsuka Electronics, Japan). Fluorescence decay curves were obtained through a fluorescence spectrometer (FLS920, Edinburgh Instruments) featuring a xenon lamp and a 450 nm pulsed laser light source. The morphology and surface structure of the samples were visualized by a SU8010 field emission scanning electron microscope (FE-SEM) (Hitachi, Japan). High-resolution transmission electron microscopy (HRTEM, FEI Tecnai F20) was implemented to inspect the nanostructure of the R-PiGs. The temperature-dependent luminescence intensity was recorded with an FL3-211-P spectrofluorometer, equipped with both a heating device and an OptistatAC-V12A cryostat system (OXFORD, Inc.). Furthermore, the laser properties of the samples, including luminous flux (LF) and luminous efficiency (LE), were evaluated by employing a HAAS-2000 optoelectronic test system (EVERFINE, China). In these tests, an LSR450CP-15W-FC blue laser served as the light source, with an operating power range of 0.15–15 W.

3 Results and discussion

The transmittance of the glass matrix plays a crucial role in influencing the performance of PiG. Therefore, the adjustment of matrix glass transmittance is essential in optimizing the properties of LuAG-PiG in laser-driven lighting [33]. Fig. 1(a) illustrates the process of glass synthesis using SPS technology, while Fig. 1(b) demonstrates the changes in the glass state during SPS sintering. Glass sintering occurs through viscous flow, wherein the deformation of initial particles increases the density of the glass [34]. As depicted, the glass in its initial state exhibits particles with a uniformly distributed shape. At temperatures below 248 ℃, the particles begin to soften and fuse together. At 255 °C, the viscous flow between particles leads to the densification of the glass. After a duration of 5 min at 255 °C, the particles completely fuse, resulting in the formation of a dense, transparent glass.

Figs. 1(c) and 1(d) present photographs of samples with varying heating rates (Z1-Z6, sintering temperatures of 255 ℃) and different sintering temperatures (Z7-Z12, heating rates of 40 ℃/min), respectively. Figs. 1(e) and 1(f) display the transmittance

curves of the samples shown in Figs. 1(c) and 1(d), respectively. When the sintering rate is set at 100 ℃/min, the sample (Z6) exhibits low transmittance, likely due to the excessively rapid sintering rate, which hinders the full fusion of the powder during the sintering process. However, at a sintering rate of 5 ℃/min, the sample (Z1) demonstrates high transmittance, despite its edges not transforming into glass. Figs. 1(c) and 1(e) indicate that a sintering rate of 40 ℃/min can yield the highest transmittance (sample Z3) when the sintering temperature is set at 255℃. Apart from the heating rate, the sintering temperature serves as another crucial parameter for achieving high transmittance. When the heating rate is 40 ℃/min and the sintering temperature is 245 ℃, the sample fails to form glass, resulting in low transmittance, as displayed in Fig. 1(f). Furthermore, samples sintered at 258 ℃ exhibit lower transmittance compared to those sintered at temperatures ranging from 250 to 255 ℃. This disparity is potentially attributable to high sintering temperatures causing carbon penetration during the melting process. Consequently, to produce efficient PiG samples, the optimal sintering conditions were determined to be a heating rate of 40 ℃/min and a sintering temperature of 255 ℃, with the corresponding sintering parameters depicted in Fig. 1(g).

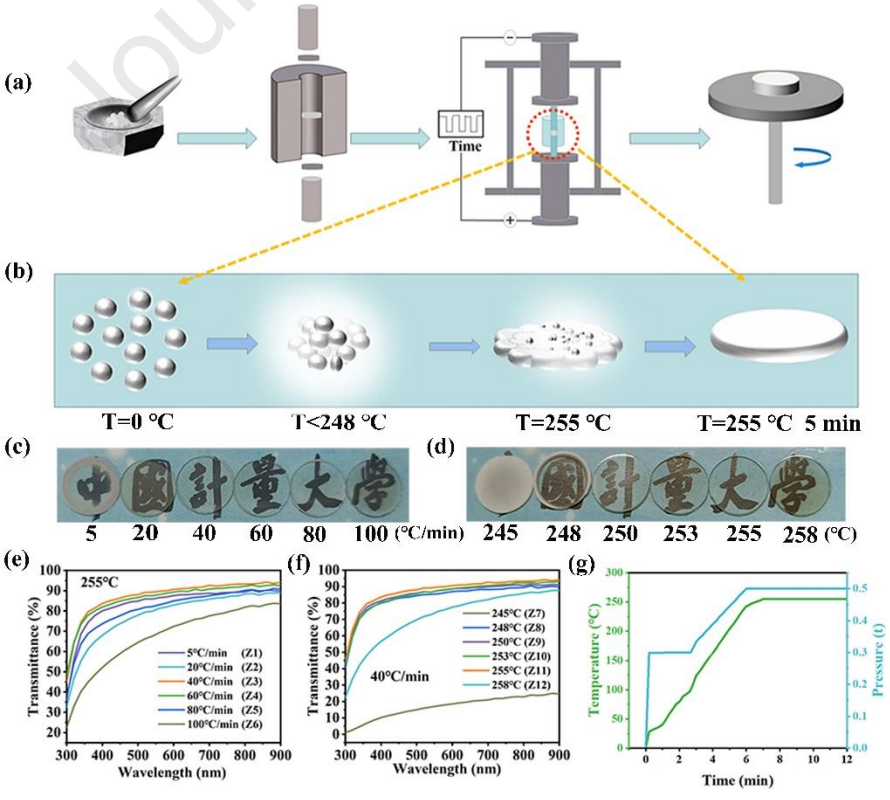

Fig. 1. (a) Process diagram illustrating the preparation of ZBLAN glass using SPS. (b) State of the glass powder at different temperatures. Photos of samples showing (c) different heating rates and (d) various sintering temperatures. (e) and (f) Transmittance curves of Z1-Z12 samples are depicted. (g) Plot illustrating the SPS procedure for the Z11 sample.

Fig. 2(a) presents digital images depicting LuAG-PiG samples with varying doping concentrations (1%–10%) under irradiation from daylight and 365 nm UV light. As the concentration of LuAG increases, the sample color gradually intensifies, resembling that of the phosphor. Consequently, LuAG-PiG emits more pronounced green light when excited by UV light. Despite the high transparency exhibited by ZBLAN glass (92% at 700 nm), the overall transmittance of LuAG-PiG experiences a notable decrease upon the introduction of LuAG doping (see Fig. 2(b)). This reduction can be predominantly attributed to Mie scattering, which is primarily influenced by the difference in refractive index (n) between the phosphors (n : 1.7 ~ 2.0) and the ZBLAN glass matrix (n : 1.4 ~ 1.6). It is important to note that the refractive index of ZBLAN glass does not significantly deviate from that of the commonly used SiO_2-B_2O_3 glass system (n : 1.5 ~ 1.7) for laser-driven lighting applications [35]. In addition, the utilization of SPS technology offers the potential for achieving complete densification under specific pressures and relatively low temperatures. This capability is advantageous for effectively controlling scattering phenomena and enhancing the management of optical properties within the material. Consequently, even with an increase in phosphor concentration up to 10%, the transmittance of the prepared ZBLAN PiG sample can still approach approximately 40%, which is comparable to certain other PiGs or phosphors-in-ceramics [22, 36]. Notably, prominent absorption bands at 450 nm appear in the transmission spectra of LuAG-PiG, originating from the 4f → 5d transitions of Ce^{3+}. XRD patterns of LuAG-PiGs demonstrate a good match with the PDF#18–0761, with no observable presence of impurity phases. The diffraction peak in the XRD pattern increases with the content of the LuAG phosphor, indicating the well-preserved cubic crystal structure of LuAG, seemingly unaffected by the glass matrix. To assess potential corrosion between the phosphor and the glass

matrix, the microstructure of the PiG samples was investigated.

High-resolution transmission electron microscopy (HRTEM) images (Fig. 2(c)) provide clear insights into the nanoscale boundary between the amorphous glass matrix and crystalline LuAG particles. Notably, the lattice stripe's plane spacing measures 0.193 nm, consistent with the (532) plane of the LuAG phosphor. The corresponding Fast Fourier Transform (FFT) pattern reveals discernible crystal points and amorphous rings, aligning with LuAG particles and the glass matrix, respectively. These results strongly suggest the absence of significant interfacial reactions between the glass matrix and the phosphors, confirming minimal corrosion of the phosphors by the glass substrate.

The Scanning Electron Microscope (SEM) image in Fig. 2(d) illustrates that the LuAG fluorescent particles exhibit spherical morphology (15-20 μm) and uniform dispersion within the glass matrix. It indicates that there was no substantial alteration in grain size and shape of LuAG during the sintering process. The corresponding element mapping images indicate that the signals corresponding to Ba, F, and Zr emanate from the glass matrix, while signals for Al, Lu, and O originate from the particles. Furthermore, a distinct boundary between the phosphor and the glass matrix is evident, consistent with the observations from HRTEM. It is noteworthy that the precise control of the SPS sintering procedure prevents significant migration of F ions, which are known to exhibit high reactivity with phosphors. This confirms that PiG, based on a multi-component glass matrix containing alkali or alkaline earth metals, can still maintain excellent interfacial morphology with phosphors through the SPS process.

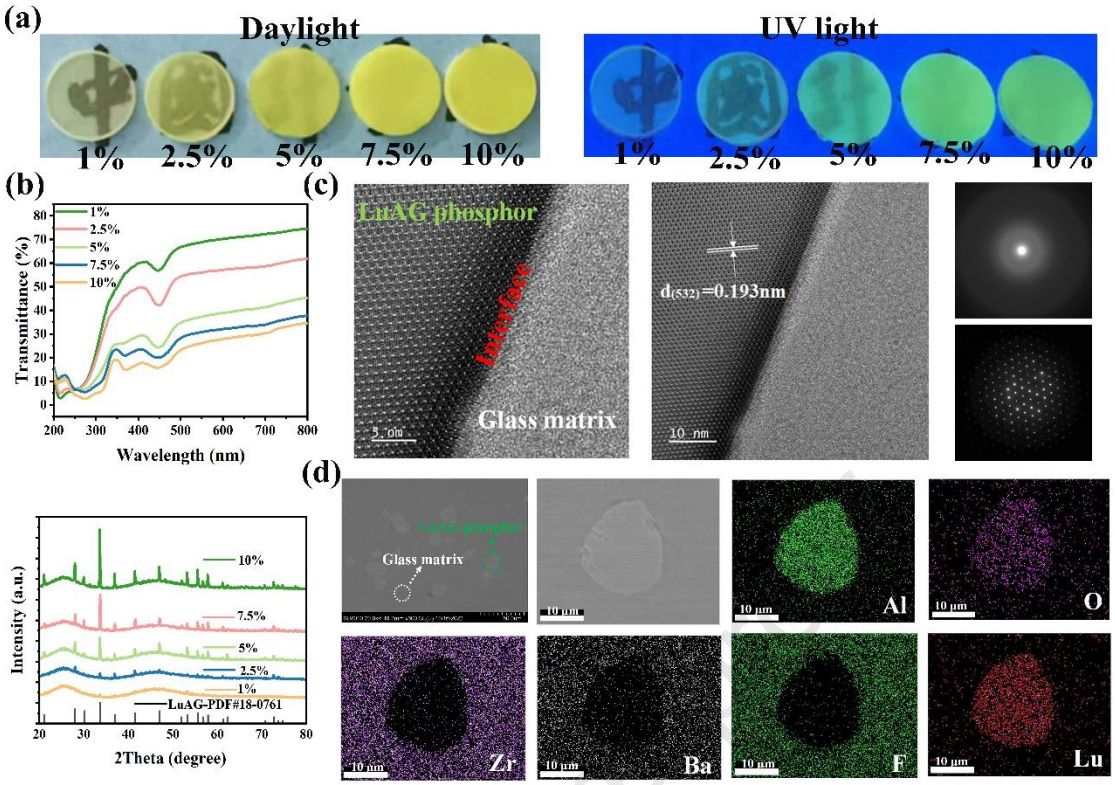

Fig. 2. Images of LuAG-PiGs with varying phosphor content (ranging from 1% to 10%) under different lighting conditions. (a) Daylight and 365 nm UV light. (b) Transmittance spectra and XRD patterns of LuAG-PiGs. (c) HRTEM images and the corresponding selected area electron diffraction (SAED) pattern. (d) SEM image along with the corresponding energy-dispersive X-ray spectroscopy (EDS) mapping specifically for the 7.5% LuAG-PiG sample.

Fig. 3(a) depicts the emission spectrum of LuAG-PiGs when subjected to 450 nm light excitation. The emission peak of LuAG reveals broadband emission spanning from 450 nm to 700 nm, and the emission intensity gradually increases with the phosphor concentration. In Fig. 3(b), the internal quantum efficiency (IQE) and external quantum efficiency (EQE) of the 7.5% LuAG-PiG sample are observed to be lower compared to the original phosphor. This discrepancy can be attributed to the variation in absorption between the glass matrix and phosphors [37, 38]. Nonetheless, the IQE and EQE values of PiG still attain 89.7% and 69.5%, respectively, thereby demonstrating the suitability of the LuAG-PiG converter for high-brightness laser-driven lighting. Furthermore, Fig. 3(c) illustrates the fluorescence lifetime of both LuAG phosphor and LuAG-PiG, measuring 57.56 ns and 56.35 ns, respectively. The

decay behaviors of the LuAG phosphor and LuAG-PiG are nearly indistinguishable, thereby reaffirming that the glass matrix and sintering process have minimal impact on the optical properties of the phosphor, consistent with TEM, EDS mapping, and XRD results.

In practical applications, the generation of heat during the laser light conversion process is inevitable and can readily elevate the operating temperature of PiG to 150 °C or even higher [23]. Consequently, the thermal performance of PiG assumes critical importance. To assess the thermal quenching performance of both LuAG phosphor and LuAG-PiG, temperature-dependent 2D fluorescence spectra were acquired under 450 nm excitation, as depicted in Figs. 3(d) and (e). As the temperature rises from 313 K to 473 K, the fluorescence intensity of the phosphor and PiG progressively diminishes, owing to the temperature-induced increase in non-radiative transition [39-41]. Simultaneously, the emission peak shifts towards longer wavelengths with rising temperature, a phenomenon attributed to thermally activated phonon-assisted tunneling [22, 42]. The normalized PL intensities of LuAG phosphor and LuAG-PiG are presented in Fig. 2(f). Remarkably, LuAG-PiG exhibits superior thermal stability when compared to LuAG phosphor, with the integrated emission intensity maintaining 94.5% of the initial value even at 473 K. These findings establish that the thermal stability of LuAG-PiG surpasses that of LuAG phosphor. Consequently, the SPS process can effectively produce PiG with outstanding optical properties based on fluoride glasses, even in the presence of F ions, known for their high reactivity with phosphors.

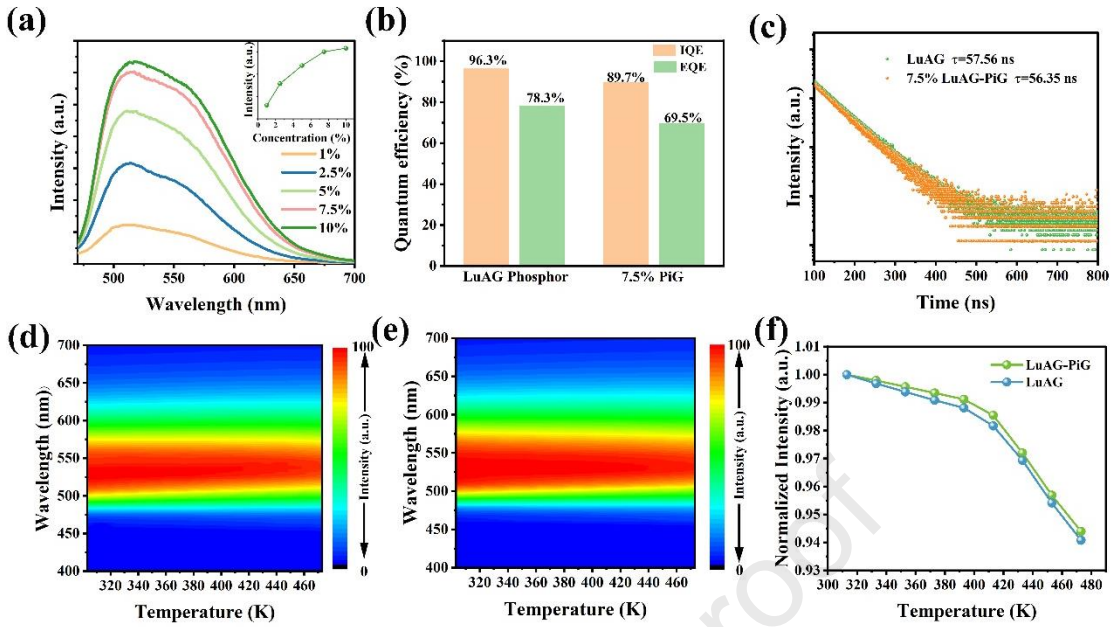

Fig. 3. (a) Photoluminescence (PL) spectra of LuAG-PiGs under 450 nm light excitation. (b) Internal quantum efficiency (IQE) and external quantum efficiency (EQE) comparison between 7.5% LuAG-PiG and LuAG phosphor powder. (c) Luminescent decay curves of 7.5% LuAG-PiG and LuAG phosphor powder. Temperature-dependent PL spectra of (d) LuAG phosphor and (e) 7.5% LuAG-PiG. (f) Normalized integrated PL intensities of LuAG phosphor and 7.5% LuAG-PiG.

To evaluate the suitability of LuAG-PiG for laser-driven lighting applications, the optical characteristics of LuAG-PiGs were assessed using a reflective configuration coupled with a 450 nm blue laser, as depicted in Fig. 4(a). Fig. 4(b) presents the PL spectra of LuAG-PiG under 450 nm blue laser excitation, showcasing typical broadband green luminescence in the range of 450-650 nm. The luminous flux (LF) and luminous efficiency (LE) of LuAG-PiG samples with varying phosphor concentrations were analyzed as the laser power varied, as illustrated in Figs. 4(c) and (d), respectively. Initially, the luminous flux (LF) exhibited a linear relationship with the incident laser power but sharply declined after reaching its peak value. This decline is a common phenomenon observed in laser-driven lighting due to the accumulation of significant heat within the color converter [21]. The luminous efficiency displayed a gradual decrease prior to reaching luminescence saturation. Notably, at a phosphor concentration of 7.5%, the maximum luminous efficiency of LuAG-PiG reached 242

lm/W even without the use of a heat sink. Additionally, the luminous flux reached 597 lm at a laser power of 2.64 W, as shown in Fig. 4(e). These results demonstrate that the LuAG-PiG, even when hosted within the highly reactive ZBLAN glass, can be fabricated through the SPS process and exhibit excellent optical properties. This highlights the potential of using stable glass compositions for PiG fabrication.

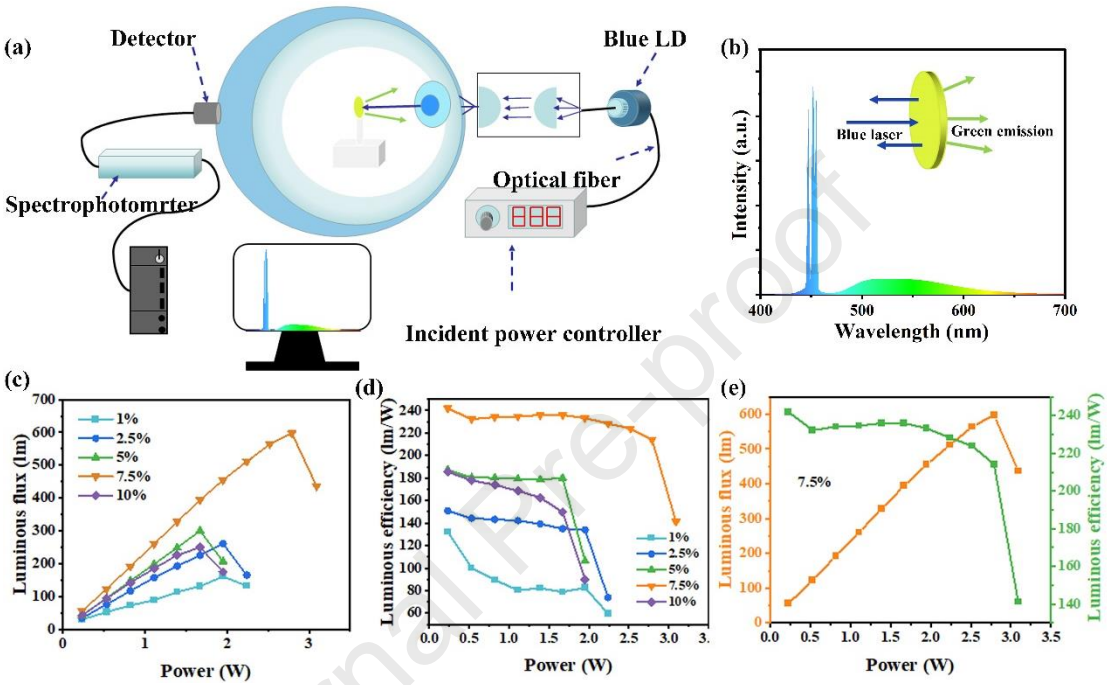

Fig. 4. (a) Schematic of the laser-driven lighting measurement device. (b) PL spectra of LuAG-PiG excited by a 450 nm blue laser. (c) LF and (d) LE of LuAG-PiG with varying phosphor concentrations (1 mm) as a function of laser power. (e) LF and LE of 7.5% LuAG-PiG as a function of the incident laser power.

Although LuAG serves as the primary green emission material with a broad PL band and a sufficient cyan component for achieving white light, it alone does not provide a high color rendering index (Ra) or a low correlated color temperature (CCT) in LD white lighting (wLD) devices. To address this limitation, a $CaAlSiN_3$: Eu^{2+} (CASN) red phosphor was incorporated as a red-light source. Various wLD devices were prepared using different 7.5% LuAG-xCASN ratios (x = 0.25%, 0.3%, 0.35%, 0.4%, 0.45%). The optical performance of wLD devices with varying CASN content was evaluated under different laser powers, as depicted in Fig. 5. Initially, the luminous flux of the wLD devices exhibited a linear increase with the laser power, but it decreased rapidly

once the laser power reached saturation (Fig. 5(a)). This saturation phenomenon is attributed to the thermal quenching process resulting from the accumulation of temperature within the sample under prolonged high-power laser excitation [21]. At a laser power of 0.353 W, the wLD device with a CASN concentration of 0.35% demonstrated the maximum luminous efficiency, reaching 210 lm/W (Fig. 5(b)). In contrast to the luminous flux and luminous efficiency, the CCT and Ra exhibited minimal changes prior to laser saturation (Fig. 5(c) and 5(d)). As a result, wLD devices with a CASN concentration of 0.35% exhibited high luminous efficiency, high Ra, and low CCT.

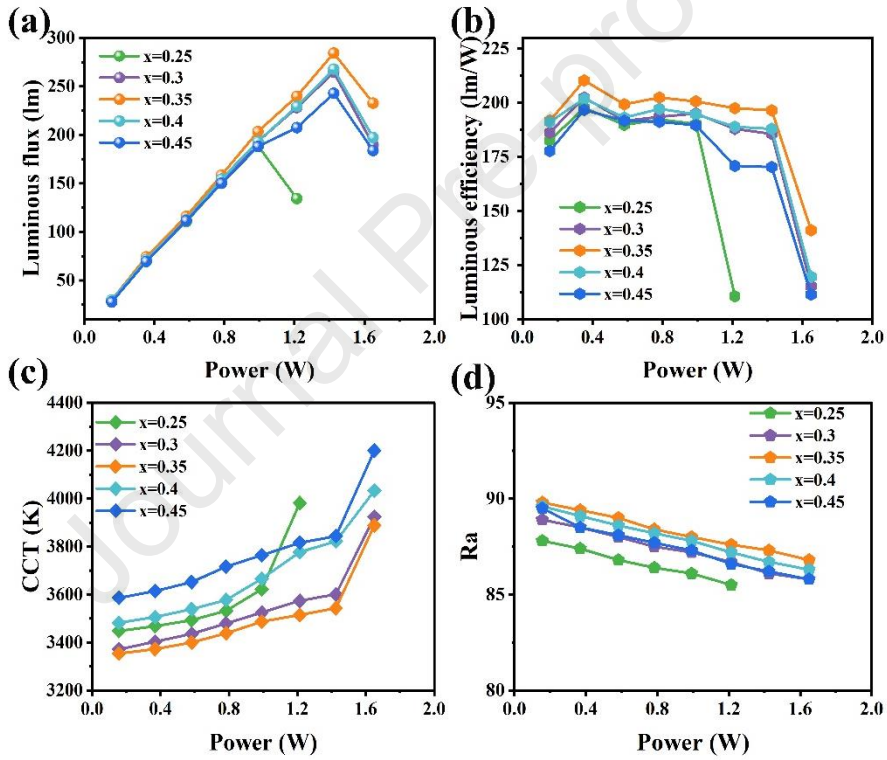

Fig. 5. (a) Luminous flux, (b) Luminous efficiency, (c) CCT, and (d) Ra of LuAG&CASN-PiGs wLD devices with the various CASN content under various laser powers.

In Fig. 6(a), we present the PL spectra of wLD devices with varying CASN concentrations, measured at a laser power of 1 W. Notably, the strongest luminous intensity is observed when the CASN concentration is at 0.35%. To further investigate the behavior of the wLD devices, Fig. 6(b) illustrates the relationship between Ra and CCT with laser power when the CASN concentration is set at 0.35%. As the power

increases, CCT rises from 3354 to 3487 K. Simultaneously, the corresponding CRI decreases from 89.8 to 88, which can be attributed to the thermal quenching process caused by the accumulated temperature in the sample under sustained high-power laser excitation. Moreover, Fig. 6(c) illustrates the CIE color coordinate diagram of the wLD devices at different power levels. As the driving power increases from 0.156 to 1.65 W, the CIE coordinates shift from (0.3827, 0.3375) to (0.3742, 0.3294). The changes in Δx and Δy are merely 0.0085 and 0.0081, respectively, which indicates that the wLD device with a CASN concentration of 0.35% demonstrates excellent color stability. In Fig. 6(d), we present the spectra of LuAG&0.35% CASN-PiG when irradiated by a 450 nm laser. The spectra exhibit broad emission ranging from 470 to 700 nm, offering a wide spectral coverage. To exemplify the practical application of the device, a photo of an LD flashlight composed of LuAG&0.35% CASN-PiG and a 450 nm laser diode is shown. To emphasize the improved color quality achieved by the flashlight, Fig. 6(e) displays a color wheel illuminated by the flashlight. The illustration clearly demonstrates that the color appears more vivid and realistic under the illumination of this flashlight. Furthermore, Fig. 6(f) showcases the illumination capability of the prepared flashlight, highlighting its ability to effectively illuminate patterns within a 5-meter distance. These results indicate that the developed PiG holds promise for a wider range of applications in the field of lighting, showcasing its potential as a versatile lighting solution.

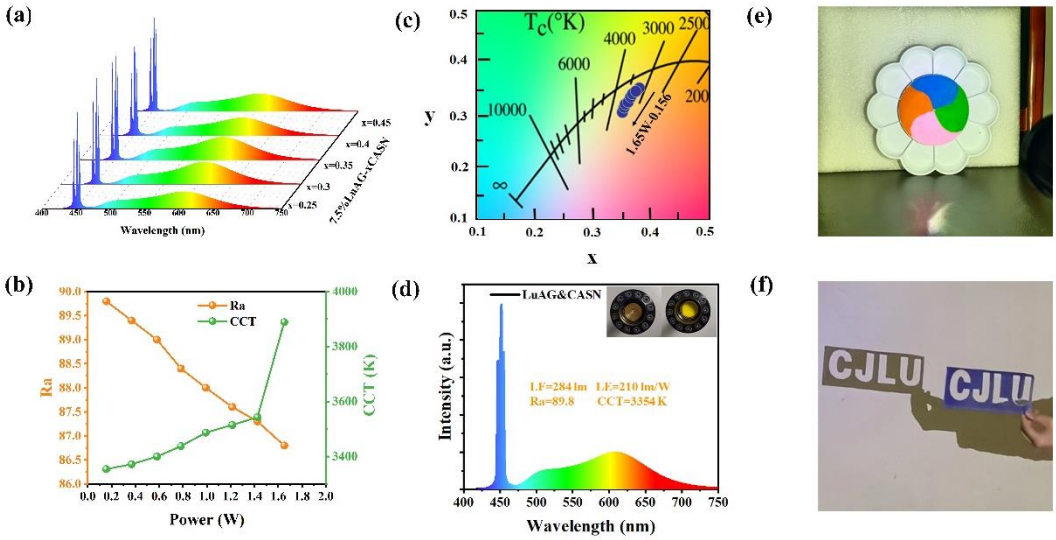

Fig. 6. (a) PL spectra of wLD devices with varying CASN content at a laser power of 1 W. (b) Variation of CCT and Ra with change in laser power. (c) CIE color coordinate diagram of wLD devices at different power. (d) Summary graph illustrating the laser performance of LuAG&0.35% CASN-PiG. (e) Photograph of color plates. (f) Photo of object illuminated by flashlights within a five meter distance.

4 Conclusion

In conclusion, the experimental findings confirmed that precise control over the sintering process through SPS enables the fabrication of high-performance PiGs, even when employing a glass matrix that is highly reactive to phosphors. This control effectively restricted the interfacial reaction between the phosphor and the glass matrix, resulting in superior PiG performance. The prepared LuAG-PiGs sample achieved an impressive luminous flux of 597 lm and a high luminous efficiency of 242 lm/W under blue laser irradiation, which is competitive within the realm of fluoride-based PiGs. Furthermore, by incorporating CASN red phosphor, wLD devices with exceptional characteristics were achieved. These devices exhibited a high luminous efficiency of 210 lm/W, a high color rendering index of 89.8, and a low color temperature of 3354 K. This work demonstrates the excellent interface morphology of PiGs prepared using the SPS low-temperature rapid sintering strategy. Consequently, this strategy holds significant promise as an effective approach for synthesizing efficient PiGs and expanding the range of glass matrix systems for high-quality laser-driven lighting. The findings presented here provide valuable insights for future research endeavors focused on laser-driven lighting.

Declaration of competing interest

We declare that we do not have any commercial or associative interest that could have appeared to influence the work reported in this paper.

Acknowledge

This research was supported by National Natural Science Foundation of China (62205321); Natural Science Foundation of Zhejiang Province (Q21F050026); The Fundamental Research Funds for the Provincial Universities of Zhejiang (2022YW32).

References

[1] 1 M. He, J. Jia, J. Zhao, X. Qiao, J. Du, X. Fan, Glass-ceramic phosphors for solid state lighting: A review, Ceram. Int. 47 (2021) 2963-2980.

[2] P. Pust, P.J. Schmidt, W. Schnick, A revolution in lighting, Nat Mater. 14 (2015) 454-8.

[3] G.J. Hoerder, M. Seibald, D. Baumann, T. Schroder, S. Peschke, P.C. Schmid, T. Tyborski, P. Pust, I. Stoll, M. Bergler, C. Patzig, S. Reissaus, M. Krause, L. Berthold, T. Hoche, D. Johrendt, H. Huppertz, $Sr[Li_{(2)}Al_{(2)}O_{(2)}N_{(2)}]:Eu^{(2+)}$-A high performance red phosphor to brighten the future, Nat Commun. 10 (2019) 1824.

[4] Y. Wei, G. Xing, K. Liu, G. Li, P. Dang, S. Liang, M. Liu, Z. Cheng, D. Jin, J. Lin, New strategy for designing orangish-red-emitting phosphor via oxygen-vacancy-induced electronic localization, Light Sci Appl. 8 (2019) 15.

[5] M. Zhao, H. Liao, M.S. Molokeev, Y. Zhou, Q. Zhang, Q. Liu, Z. Xia, Emerging ultra-narrow-band cyan-emitting phosphor for white LEDs with enhanced color rendition, Light Sci Appl. 8 (2019) 38.

[6] J. Cho, E.F. Schubert, J.K. Kim, Efficiency droop in light-emitting diodes: Challenges and countermeasures, Laser Photonics Rev. 7 (2013) 408-421.

[7] N. Trivellin, M. Yushchenko, M. Buffolo, C. De Santi, M. Meneghini, G. Meneghesso, E. Zanoni, Laser-Based Lighting: Experimental Analysis and Perspectives, Materials (Basel). 10 (2017).

[8] J.J. Wierer, J.Y. Tsao, D.S. Sizov, Comparison between blue lasers and light-emitting diodes for future solid-state lighting, Laser Photonics Rev. 7 (2013) 963-993.

[9] P. Zheng, S. Li, R. Wei, L. Wang, T.L. Zhou, Y.R. Xu, T. Takeda, N. Hirosaki, R.J. Xie, Unique Design Strategy for Laser-Driven Color Converters Enabling Superhigh-Luminance and High-Directionality White Light, Laser Photonics Rev. 13 (2019).

[10] Q. Huang, P. Sui, F. Huang, H. Lin, B. Wang, S. Lin, P. Wang, J. Xu, Y. Cheng, Y. Wang, Toward High-Quality Laser-Driven Lightings: Chromaticity-Tunable

Phosphor-in-Glass Film with “Phosphor Pattern” Design, Laser Photonics Rev. 16 (2022).

[11] X. Zhang, J. Yu, J. Wang, B. Lei, Y. Liu, Y. Cho, R.-J. Xie, H.-W. Zhang, Y. Li, Z. Tian, Y. Li, Q. Su, All-Inorganic Light Convertor Based on Phosphor-in-Glass Engineering for Next-Generation Modular High-Brightness White LEDs/LDs, ACS Photonics. 4 (2017) 986-995.

[12] Y. Peng, Y. Mou, H. Wang, Y. Zhuo, H. Li, M. Chen, X. Luo, Stable and efficient all-inorganic color converter based on phosphor in tellurite glass for next-generation laser-excited white lighting, J. Eur. Ceram. Soc. 38 (2018) 5525-5532.

[13] Y. Zhou, C. Yu, E. Song, Y. Wang, H. Ming, Z. Xia, Q. Zhang, Three Birds with One Stone: $K_2SiF_6:Mn^{4+}$Single Crystal Phosphors for High-Power and Laser-Driven Lighting, Adv. Opt. Mater. 8 (2020).

[14] J. Xu, A. Thorseth, C. Xu, A. Krasnoshchoka, M. Rosendal, C. Dam-Hansen, B. Du, Y. Gong, O.B. Jensen, Investigation of laser-induced luminescence saturation in a single-crystal YAG:Ce phosphor: Towards unique architecture, high saturation threshold, and high-brightness laser-driven white lighting, J. Lumin. 212 (2019) 279-285.

[15] C. Shao, L. Zhang, T. Zhou, L. Gu, B. Sun, Z. Jiang, Q. Yao, W. Bu, K. Wang, H. Chen, Gd_2O_3 assisted densification of high quantity (Y, Gd)AG: Ce ceramic solid solutions and their luminescence characteristics, Ceram. Int. 44 (2018) 8672-8678.

[16] T.W. Kang, K.W. Park, J.H. Ryu, S.G. Lim, Y.M. Yu, J.S. Kim, Strong thermal stability of $Lu_3Al_5O_{12}:Ce^{3+}$ single crystal phosphor for laser lighting, J. Lumin. 191 (2017) 35-39.

[17] M. Rejman, V. Babin, R. Kucerková, M. Nikl, Temperature dependence of CIE-x,y color coordinates in YAG:Ce single crystal phosphor, J. Lumin. 187 (2017) 20-25.

[18] J.G. Bohnet, B.C. Sawyer, J.W. Britton, M.L. Wall, A.M. Rey, M. Foss-Feig, J.J. Bollinger, Quantum spin dynamics and entanglement generation with hundreds of trapped ions, Science. 352 (2016) 1297-301.

[19] C. Gu, X.-J. Wang, C. Xia, S. Li, P. Liu, D. Li, H. Li, G. Zhou, J. Zhang, R.-J. Xie, A new CaF_2-YAG:Ce composite phosphor ceramic for high-power and high-color-

rendering WLEDs, J. Mater. Chem. C. 7 (2019) 8569-8574.

[20] J. Kang, L. Zhang, Y. Li, Y. Ma, B. Sun, Y. Liu, T. Zhou, F.A. Selim, C. Wong, H. Chen, Luminescence declining behaviors in YAG:Ce transparent ceramics for high power laser lighting, J. Mater. Chem. C. 7 (2019) 14357-14365.

[21] Q. Yao, P. Hu, P. Sun, M. Liu, R. Dong, K. Chao, Y. Liu, J. Jiang, H. Jiang, YAG:$Ce^{(3+)}$ Transparent Ceramic Phosphors Brighten the Next-Generation Laser-Driven Lighting, Adv Mater. 32 (2020) e1907888.

[22] L. Wang, H. Yang, Y. Zhang, Y. Liang, J. Zhang, E. Mei, F. Xu, J. Long, P. Yu, W. Xiang, All-inorganic high efficiency LuAG:Ce^{3+} converter based on phosphor-in-glass for laser diode lighting, J. Alloys Compd. 892 (2022).

[23] Q. Li, W. Xiao, D. Zhang, D. Wang, G. Zheng, J. Qiu, Phosphor-in-Silica-Glass: Filling the Gap between Low- and High-Brightness Solid-State Lightings, Laser Photonics Rev. 16 (2022).

[24] D. Han, D.S. Li, Y.J. Zhang, H. Lin, E.Y.B. Pun, Crystalline-phase depuration in Ce^{3+} activated $Lu_3Al_5O_{12}$-tellurite green-emitting phosphor-in-glass, J. Lumin. 214 (2019).

[25] R. Wei, L. Wang, P. Zheng, H. Zeng, G. Pan, H. Zhang, P. Liang, T. Zhou, R. Xie, On the luminance saturation of phosphor-in-glass (PiG) films for blue-laser-driven white lighting: Effects of the phosphor content and the film thickness, J. Eur. Ceram. Soc. 39 (2019) 1909-1917.

[26] H. Yang, Y. Zhang, Y. Zhang, Y. Zhao, X. Liang, G. Chen, Y. Liu, W. Xiang, Designed glass frames full color in white light-emitting diodes and laser diodes lighting, Chem. Eng. J. 414 (2021).

[27] H.L. Fang, S.J. Gu, S.J. Fan, B.Y. Zhou, P. Huang, W. Luo, L.J. Wang, W. Jiang, Rapidly fabricating Y_2O_3 transparent ceramics at low temperature by SPS with mesoporous powder, J. Am. Ceram. Soc. 106 (2023) 2491-2500.

[28] B.Y. Zhou, W. Luo, S. Liu, S.J. Gu, M.C. Lu, Y. Zhang, Y.C. Fan, W. Jiang, L.J. Wang, Enhancing the performance of Ce:YAG phosphor-in-silica-glass by controlling interface reaction, Acta Mater. 130 (2017) 289-296.

[29] D. Zhang, W. Xiao, C. Liu, X. Liu, J. Ren, B. Xu, J. Qiu, Highly efficient phosphor-

glass composites by pressureless sintering, Nat Commun 11 (2020) 2805.

[30] S. Arjoca, E.G. Víllora, D. Inomata, K. Aoki, Y. Sugahara, K. Shimamura, "Ce:(Y1-xLux)$_3$Al$_5$O$_{12}$ single-crystal phosphor plates for high-brightness white LEDs/LDs with high-color rendering (Ra > 90) and temperature stability," Mater. Res. Express. 1 (2014) 025041.

[31] Y. Zhang, Y. Liang, Y. Zhang, X. Liu, Y. Yu, Y. Zhao, X. Liang, W. Xiang, "High color rendering index composite phosphor-in-glass for high-power white laser lighting," J. Eur. Ceram. Soc. 41 (2021) 4915–4923.

[32] S.A. Cicillini, A.M. Pires, O.A. Serra, "Luminescent and morphological studies of Tm-doped Lu$_3$Al$_5$O$_{12}$ and Y$_3$Al$_5$O$_{12}$ fine powders for scintillator detector application," J. Alloys Compd. 374 (2004) 169-172.

[33] X. Zhang, S. Si, J. Yu, Z. Wang, R. Zhang, B. Lei, Y. Liu, J. Zhuang, C. Hu, Y. Cho, R.-J. Xie, H.-W. Zhang, Z. Tian, J. Wang, Improving the luminous efficacy and resistance to blue laser irradiation of phosphor-in-glass based solid state laser lighting through employing dual-functional sapphire plate, J. Mater. Chem. C. 7 (2019) 354-361.

[34] G. Delaizir, Y. Gueguen, M. Hubert, X.H. Zhang, J. Monnier, C. Godart, L. Calvez, L. Pinckney, Investigation of the Mechanisms Involved in the Sintering of Chalcogenide Glasses and the Preparation of Glass-Ceramics by Spark Plasma Sintering, J. Am. Ceram. Soc. 95 (2012) 2211-2217.

[35] J. Seo, S. Kim, Y. Kim, F. lqbal, H. Kim, A. Setlur, Effect of Glass Refractive Index on Light Extraction Efficiency of Light-Emitting Diodes, J. Am. Ceram. Soc. 97 (2014) 2789-2793.

[36] M. Zhou, J. Sun, B. Zhang, Y. Hua, F. Huang, H. Ma, R. Ye, S. Xu, Ultra-high efficiency green-emitting LuAG: Ce phosphor-in-ceramic applied for high-power laser lighting, J. Eur. Ceram. Soc. 43 (2023) 3563-3571.

[37] S.H. Ahn, Y.H. Nam, K. Han, W.B. Im, K.Y. Cho, W.J. Chung, Phosphor-in-glass thick film formation with low sintering temperature phosphosilicate glass for robust white LED, J. Am. Ceram. Soc. 100 (2017) 1280-1284.

[38] Q.-Q. Zhu, X. Xu, L. Wang, Z.-F. Tian, Y.-Z. Xu, N. Hirosaki, R.-J. Xie, A robust

red-emitting phosphor-in-glass (PiG) for use in white lighting sources pumped by blue laser diodes, J. Alloys Compd. 702 (2017) 193-198.

[39] Y. Liu, J. Silver, R.-J. Xie, J. Zhang, H. Xu, H. Shao, J. Jiang, H. Jiang, An excellent cyan-emitting orthosilicate phosphor for NUV-pumped white LED application, J. Mater. Chem. C. 5 (2017) 12365-12377.

[40] Y. Liu, J. Zhang, C. Zhang, J. Xu, G. Liu, J. Jiang, H. Jiang, $Ba_9Lu_2Si_6O_{24}:Ce^{3+}$: An Efficient Green Phosphor with High Thermal and Radiation Stability for Solid-State Lighting, Adv. Opt. Mater. 3 (2015) 1096-1101.

[41] Z. Jia, C. Yuan, Y. Liu, X.J. Wang, P. Sun, L. Wang, H. Jiang, J. Jiang, Strategies to approach high performance in $Cr^{(3+)}$-doped phosphors for high-power NIR-LED light sources, Light Sci Appl. 9 (2020) 86.

[42] Y. Xu, S. Li, P. Zheng, L. Wang, S. You, T. Takeda, N. Hirosaki, R.-J. Xie, A search for extra-high brightness laser-driven color converters by investigating thermally-induced luminance saturation, J. Mater. Chem. C. 7 (2019) 11449-11456.

We declare that we do not have any commercial or associative interest that could have appeared to influence the work reported in this paper.